n-Heptane oxidation in a high-pressure flow reactor

Thorsen, Lauge Sven; Jensen, Malene Stryhn Thestrup; Pullich, Mille Stub; Christensen, Jakob Munkholt; Hashemi, Hamid; Glarborg, Peter

Published in:
International Journal of Chemical Kinetics

Link to article, DOI:
10.1002/kin.21604

Publication date:
2022

Document Version
Publisher's PDF, also known as Version of record

Received: 5 April 2022 | Revised: 8 July 2022 | Accepted: 30 July 2022

DOI: 10.1002/kin.21604

INTERNATIONAL JOURNAL OF CHEMICAL KINETICS | WILEY

RESEARCH ARTICLE

n-Heptane oxidation in a high-pressure flow reactor

Lauge Sven Thorsen | **Malene Stryhn Thestrup Jensen** | **Mille Stub Pullich** | **Jakob Munkholt Christensen** | **Hamid Hashemi** | **Peter Glarborg**

DTU Chemical Engineering, Technical University of Denmark, Lyngby, Denmark

Correspondence
Peter Glarborg, DTU Chemical Engineering, Technical University of Denmark, Lyngby DK-2800, Denmark.
Email: pgl@kt.dtu.dk

Funding information
Det Frie Forskningsråd

Abstract

The oxidation properties of *n*-heptane have been investigated by conducting experiments in a laminar flow reactor at pressures of 21 and 100 bar, near-stoichiometric ($\Phi = 0.9$) and fuel-lean conditions ($\Phi = 0.1$), and temperatures of 450–900 K. At 21 bar and stoichiometric conditions, a negative temperature coefficient (NTC) region was detected around 600 K. At increased pressure or oxygen concentration, the NTC behavior was much less pronounced. The observed concentration profiles for the major species were compared to predictions with selected literature mechanisms. While all models provided a satisfactory agreement for the *n*-heptane profiles at 21 bar fuel lean conditions and at 100 bar, only the mechanisms from NUI and Polimi captured the NTC behavior at 21 bar and stoichiometric conditions. The model from Zhang et al. provided the best overall agreement and was selected for detailed comparison with species concentrations and used in analysis of reaction paths and reaction sensitivity under the present conditions.

KEYWORDS
flow reactor experiments, heptane, high pressure, kinetic modeling, oxidation

1 | INTRODUCTION

n-Heptane is often used as a surrogate fuel for diesel as it exhibits similar combustion properties, that is, it has the same cetane number (CN) and burning velocity. The *n*-heptane oxidation involves both low and high temperature regimes. The transition region exhibits a negative temperature coefficient (NTC) as reported in literature for shock tube,[1–6] jet-stirred reactor,[7–9] rapid compression machine,[10–14] and flow reactor[15,16] experiments. The low temperature chemistry is initiated by hydrogen abstraction from *n*-heptane (RH) forming an alkyl radical (R), followed by addition of oxygen to form a peroxy radical (ROO). The peroxy radical can undergo an internal hydrogen abstraction forming a hydroperoxide alkyl radical (QOOH), which can add another O_2 molecule. The peroxide chemistry, including a range of isomers and stereochemistry as well as a large number of possible decomposition steps, is complex and challenging for kinetic modeling. Curran et al.[17] used a systematic approach including nine classes of high temperature reactions and 16 classes of low temperature reactions to generate a detailed *n*-heptane oxidation mechanism involving 550 species and 2450 reactions. In subsequent work, the *n*-heptane mechanism has been further refined by various groups. Selected models are listed in Table 1.

TABLE 1 Detailed kinetic *n*-heptane models evaluated in this study. The pressure (P), temperature (T), and fuel-air equivalence ratio (ϕ) range of validation for each model is listed

Model	Species	Reactions	*P* (bar)	*T* (K)	ϕ
Mehl et al.[18]	654	2827	3–50	650–1200	0.3–1.0
Seidel et al.[19]	349	1983	13.5–40	650–1250	0.5–3.0
Cai and Pitsch[20]	339	1690	3–42	650–1400	0.5–2.0
Zhang et al.[9]	1268	5336	6.5–55	590–1250	0.25–1.0
Wu et al.[21]	2746	11,279	13.5–55	590–1250	0.25–1.0
Ranzi and coworkers[22–25]	339	9781	1–60	800–1700	0.1–3

The detailed kinetic models were all evaluated by comparing predictions with ignition delay times (IDT) from shock tube and rapid compression machines. The ignition delay data cover a wide range of pressure (3–55 bar), temperature (590–1400 K), and fuel–air equivalence ratio (0.25–3.0) (Table 1). No data are available for pressures above 65 bar.[26] Other results used in model validation were all obtained at pressures well below those of engines; they include jet-stirred reactor experiments[8,9] at pressures of 1–10 bar and laminar flame speed data,[27,28] obtained at atmospheric pressure.

Flow reactors are also suitable to investigate the oxidation properties of *n*-heptane. Held et al.[29] measured in situ mole fractions of *n*-heptane and intermediates at 3 bar, with initial temperatures in the range 940–1085 K. At the lower temperatures relevant for the NTC behavior, species profiles were reported by Callahan et al.[15] (550–800 K and 12.5 bar) and Lenhert et al.[16] (600–800 K and 8 bar).

It is important to supplement the high-pressure IDT data with species profiles from high-pressure flow reactor experiments to provide the basis for further model refinement under conditions relevant for engine simulations. Thus, this study presents results from laminar flow reactor experiments conducted at 21 and 100 bar, temperatures of 450–900 K, and both at near-stoichiometric and lean conditions. The experimental data are compared to predictions with the detailed kinetic *n*-heptane models listed in Table 1. The mechanism of Zhang et al.,[9] which provides the best overall agreement with experiment, is selected for detailed comparison with species concentrations and used in analysis of reaction paths and reaction sensitivity under the present conditions.

2 | METHODS

2.1 | Experimental setup

The high-pressure flow reactor at the Technical University of Denmark (DTU) is designed to operate at pressures up to 100 bar. The setup is described in detail elsewhere[30,31] and only a brief description is given here. The reactor is a 154-cm long quartz tube with 8-mm inner diameter. Surrounding the quartz tube, a steel container acting as a pressure shell isolates a pressurized cavity that prevents large pressure gradients over the quartz tube. A moveable thermostat is placed inside the steel container to estimate the temperature inside the reactor. The reactor is pressurized using a Baumann 51000 Low Flow Control Valve, and the pressure shell is pressurized using Brooks 5866 Compact Pressure Controllers. Heating trace (~373 K) is used downstream to prevent product condensation.

High-pressure mass flow controllers (Brooks SLA5850 series) are used to control the input flow from the gas bottles of the reactant gasses (heptane and O_2) and nitrogen (for dilution). Gas bottles from Air Liquid with certified concentrations of ±2% were used. The total mass flow was maintained at 1400 Nml/min, allowing for a good plug-flow approximation in the laminar flow regime.[30] Temperature profiles in the reactor at inert conditions were measured as shown in Figure 1. We define the isothermal zone to be the length of the reactor where the temperature is within ±6 K, measured to be 45–48 cm at 21 bar and 39–45 cm at 100 bar. This corresponds to residence times in the isothermal zone of 6–10 s at 21 bar and 28–57 s at 100 bar, decreasing with temperature.

For product analysis and initial concentration determination, a Trace 1300/1310 gas chromatograph (GC) from Thermo Fisher was used. The GC used a Flame Ionization Detector (FID) with a capillary column Rtx-5, and a Thermal Conductivity Detector (TCD) with three micro packed columns; Rt-XLSulfur, Molsieve-5A, and HS-N (HayeSep). For every measuring temperature, two to five GC samples were collected to determine the species mole fractions with a measuring uncertainty within 10%. However, for CO (due to weak signals in the TCD caused by separation issues) and for species in very low quantities (around 1 ppm), the measuring uncertainty was above 10%. The GC was calibrated for heptane, butane, *iso*-butene, propane, propene, ethane, ethene, methane, methanol, acetaldehyde, CO, CO_2, and O_2.

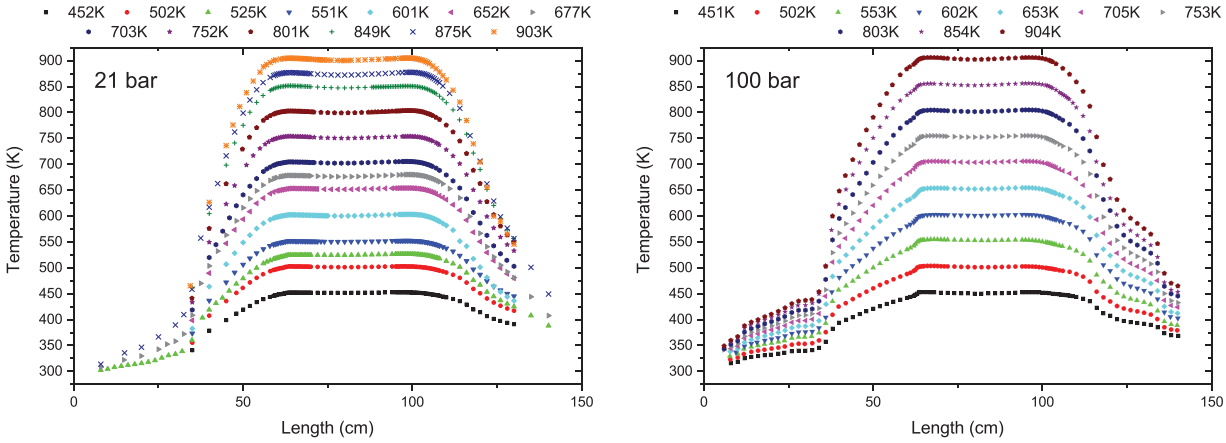

FIGURE 1 Temperature profiles of the reactor for a flow rate of ~1500 Nml/min and pressure of 21 and 100 bar, respectively

TABLE 2 Conditions for the flow reactor experiments. All experiments were conducted highly diluted in N_2. Additional details about the conditions can be found in Supplementary Material Table S1.

Experiment	Pressure bar	ϕ	*n*-Heptane ppm	Oxygen ppm
1	21	0.9	52.4	642
2	21	0.1	51.2	6395
3	100	0.9	49.3	587
4	100	0.1	50.6	5516

3 | RESULTS AND DISCUSSION

The experiments were performed in the high-pressure flow reactor at 21 and 100 bar. The oxidation was conducted at close to stoichiometric ($\phi \sim 0.9$) and fuel lean ($\phi \sim 0.1$) conditions. An overview of the experimental conditions is given in Table 2. Mole fractions of the reactants (*n*-heptane and O_2) and products (CO, CO_2, methane, methanol, ethene, acetaldehyde, propane/propene) were extracted from the GC output, and the results are shown in Figures 2–5.

The experimental results were compared with modeling predictions, assuming plug-flow conditions in the reactor. The calculations were conducted in ANSYS Chemkin-Pro[32] using the measured temperature profiles in Figure 1. Due to the high reactivity of *n*-heptane, reaction in the preheating section may contribute to the conversion and it was important to use the full temperature profile rather than just simulating the isothermal zone.

The modeling analysis was conducted in two stages. First a screening of the accuracy of recent literature mechanisms was conducted by comparing predictions to the measured *n*-heptane profiles for stoichiometric conditions at 21 and 100 bar. Next, the preferred kinetic model was used to interpret the detailed concentration profiles.

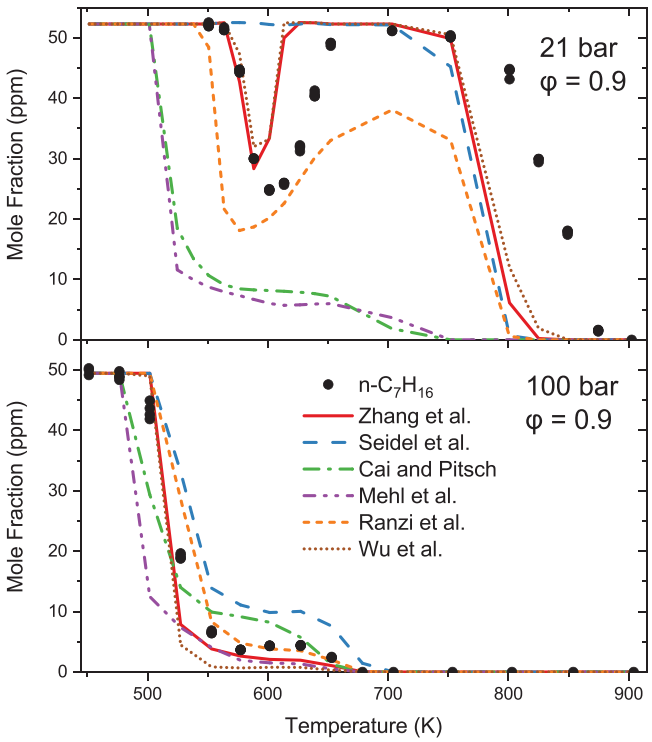

FIGURE 2 Comparison of predictions from selected kinetic models with the measured *n*-heptane mole fraction in the flow reactor experiments at stoichiometric conditions and at 21 and 100 bar. The mixture compositions are listed in Table 2. Symbols denote experimental results, while lines correspond to calculations using the models of Zhang et al.,[9] Seidel et al.,[19] Cai and Pitsch,[20] Mehl et al.,[18] Ranzi and coworkers,[22–25] and Wu et al.[21] The nominal temperature refers to the temperature profiles in Figure 1

3.1 | Screening of kinetic models

All models were evaluated against a limited set of data. Figure 2 compares the measured *n*-heptane concentration

profiles for stoichiometric conditions at 21 and 100 bar with modeling predictions. The kinetic models selected for comparison were those listed in Table 1, that is, from Zhang et al.,[9] Seidel et al.,[19] Cai and Pitsch,[20] Mehl et al.,[18] Wu et al.,[21] and Ranzi and coworkers.[22–25]

At 21 bar, the *n*-heptane concentration profile shows a strong NTC behavior. The onset of oxidation occurs at 550 K and about half of the *n*-heptane is consumed at 600 K. Above 600 K, the oxidation rate slows down, and between 650 and 750 K, little conversion of *n*-heptane is detected. At 800 K, the reaction becomes faster, and at 850 K, the *n*-heptane is fully consumed. Only the models from Zhang et al.,[9] Ranzi and coworkers,[22–25] and Wu et al.[21] are able to capture this behavior; the other models do not predict NTC behavior under these conditions. The mechanism by Seidel et al.[19] does not predict any conversion of *n*-heptane in the NTC region at 21 bar, but captures satisfactorily the onset of the high temperature oxidation at 750 K. The models by Cai and Pitsch[20] and Mehl et al.[18] strongly overpredict the low-temperature reactivity of *n*-heptane, resulting in about 80% conversion of *n*-heptane already at 550 K and full depletion at 750 K.

The model from Ranzi and coworkers[22–25] captures the location of the NTC region, but tends to overpredict the *n*-heptane consumption in the whole temperature range. The most accurate predictions are offered by the models from Curran and coworkers, that is, Zhang et al.[9] and the recent update from Wu et al.[21] (NUIGMech1.1).

At 100 bar in Figure 2, the NTC behavior is much less pronounced. Oxidation is initiated at 500 K and more than 80% of the *n*-heptane is converted at 550 K. Around 600 K, there is a weak NTC region, indicated by a shoulder in the *n*-heptane profile, and above 650 K, the *n*-heptane is depleted. The differences in predictions among the kinetic models are much smaller under these conditions. All the models capture satisfactorily the behavior with a low temperature conversion, followed by a transition region, before the *n*-heptane is fully converted in the high temperature region. Again, the most accurate predictions are offered by the models from Zhang et al.[9], Wu et al.[21], and Ranzi and coworkers.[22–25]

All mechanisms have been validated previously against ignition delay measurements from rapid compression machines in a similar temperature range and at elevated pressure. The considerable differences in modeling predictions under the current conditions support the need for the high-pressure flow reactor data to further refine and validate the models for oxidation of *n*-heptane. Overall, the model by Zhang et al.[9] offers the most accurate predictions, and this mechanism is chosen for interpretation of the detailed speciation.

3.2 | Detailed comparison with Zhang model

3.2.1 | *n*-Heptane and O_2

Figure 3 extends the experimental data in Figure 2 with fuel lean conditions and O_2 mole fractions, and compared to the model predictions by Zhang et al.[9] The onset temperature of the NTC region, where the heptane concentration starts to increase, is lowered by 25 K at increasing pressure. Either increasing the pressure from 21 to 100 bar or going to fuel lean conditions largely eliminate the NTC behavior, even though a transition region is still visible. The increased low temperature conversion of *n*-heptane at lean conditions is explained by an increased formation of peroxy radicals that enhances radical formation, as discussed below. The larger conversion of *n*-heptane at higher pressure is promoted by the increased residence time.

Also the depletion of *n*-heptane occurs at lower temperatures when increasing the pressure or oxygen concentration. Going from 21 bar and stoichiometric conditions to 100 bar and lean conditions causes a shift in the temperature for full conversion of *n*-heptane from 900 to 675 K. The observed effects of pressure, residence time, and stoichiometry are consistent with previous results in literature[7,9 15].

As expected, the oxygen consumption follows that of *n*-heptane. At the highest temperatures under lean conditions, about 500 ppm of oxygen is consumed, corresponding well to the stoichiometric ratio of 550 ppm oxygen to 50 ppm *n*-heptane. At close to stoichiometric conditions, the oxygen is not fully converted, especially at 21 bar.

A significant fraction of the carbon fed as *n*-heptane is accumulated in oxygenated derivatives that are not quantified by the GC. A carbon balance shows that up to 70% of the initial carbon is not accounted for, especially at lower temperatures (see Supplementary Material Figures S1–S3). However, when the carbon balance is extended to include predicted concentrations of the intermediates not detected, the deviation is reduced to 7% or below at lower temperatures for all conditions (see Tables S2 and S3). At higher temperatures, where *n*-heptane is largely converted to CO and CO_2, there is a ~10% deviation in the carbon balance; this can be attributed mostly to the uncertainty in the CO quantification.

Overall, the model by Zhang et al.[9] provides a good agreement with the experimental data. However, at 21 bar and stoichiometric conditions, the temperature for onset of the NTC region is underpredicted, as is the temperature for the rapid conversion above 750 K. In addition, the low temperature *n*-heptane conversion at 100 bar and lean conditions are overpredicted.

INTERNATIONAL JOURNAL OF CHEMICAL KINETICS WILEY

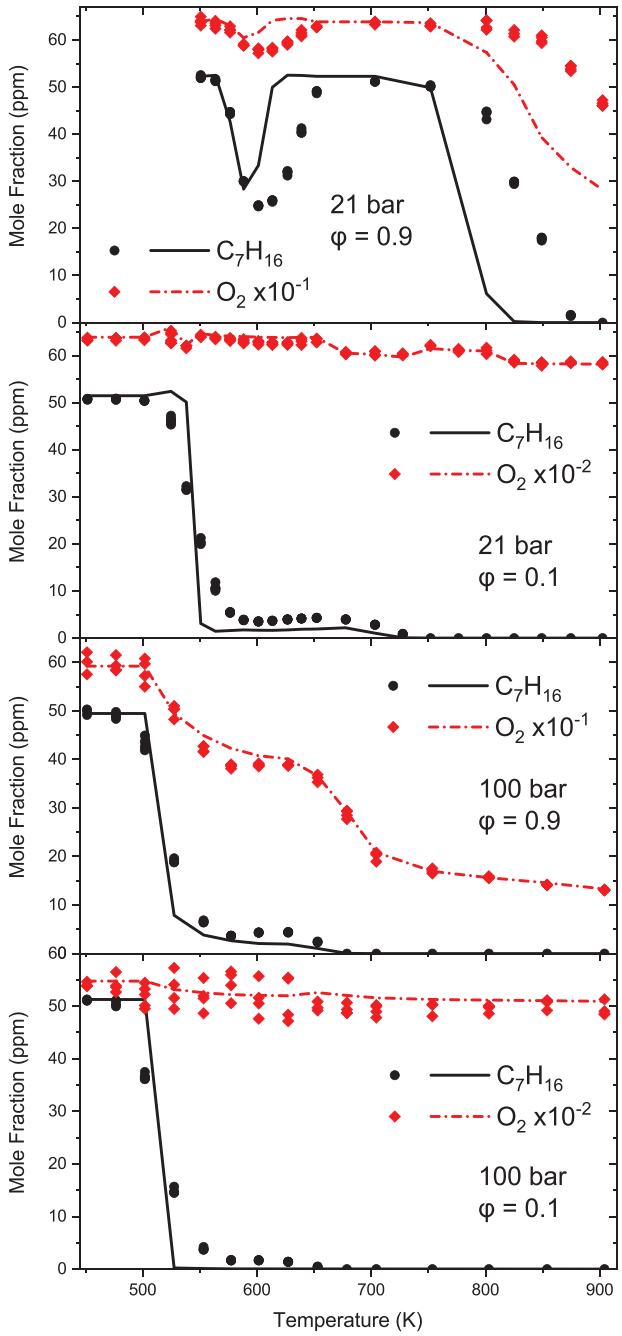

FIGURE 3 Comparison of the measured mole fractions of *n*-heptane and oxygen in the flow reactor as a function of temperature, pressure, and stoichiometry with predictions from the kinetic model of Zhang et al.[9] Symbols denote experimental results, while lines correspond to modeling predictions. Mixture compositions are listed in Table 2. The temperature refers to the temperature profiles in Figure 1

3.2.2 | Intermediates

Even though a number of larger hydrocarbons and oxygenated species could not be quantified in the present work, the GC FID signals do provide results for a range of intermediates formed during the oxidation of *n*-heptane oxidation. Figure 4 shows mole fractions of the hydrocarbon intermediates propane/propene ($C_3H_{6/8}$), ethane (C_2H_6), and ethene (C_2H_4), along with the oxygenated species acetaldehyde (CH_3CHO) and methanol (CH_3OH). The mole fractions of propane and propene are added and shown as one ($C_3H_{6/8}$) since the peaks were inseparable. Analysis of a mixture of propane and propene in known concentrations indicated that the propane and propene calibration factors are similar. Measured concentrations of C_4 species, present only in low quantities, are shown in the Supplementary Material Figure S4.

The intermediates were detected in the highest concentrations at 21 bar, near-stoichiometric conditions, and temperatures above 800 K. In the low-temperature region, hydrocarbon intermediates were detected only in very small concentrations. The most abundant species were ethene, methane, and propane/propene (mainly propene, according to the simulations). The peak levels of these hydrocarbons were in good agreement with modeling predictions. However, the concentration of C_2H_4 is generally overpredicted at lower temperatures and underpredicted above 700 K.

The C_4 species butane and iso-butene were detected in levels of 3–7 ppm (see Supplementary Material Figure S4). However, according to the kinetic model, formation of C_4 hydrocarbons is largely limited to 1-butene, which is predicted in levels of around 1 ppm. It is not clear whether the difference is due to a shortcoming of the model or to inadequate separation between species in the GC.

As the oxygen availability or pressure increases, the *n*-heptane oxidation becomes faster and occurs at lower temperature (Figure 3). For these conditions, fewer intermediates are detected. However, small amounts of propane/propene, ethene, and methane are measured at 21 bar and lean conditions, and methane was detected at 21 bar and lean conditions, and 100 bar and near-stoichiometric conditions.

In addition to hydrocarbons, methanol and acetaldehyde were detected. These intermediates were mainly formed in the low temperature region between 500 and 700 K. The largest mole fractions of methanol were observed at 100 bar and stoichiometric conditions while acetaldehyde formation was most pronounced at 21 bar and lean conditions. Small amounts of acetaldehyde were also formed in the high temperature region at 21 bar and stoichiometric conditions. The measured levels of ethene and acetaldehyde at 21 bar lean conditions are consistent with the study of Lenhert et al.[16] The concentration of acetaldehyde is predicted within a factor of two or better, while methanol formation is overpredicted by factors of 2–5.

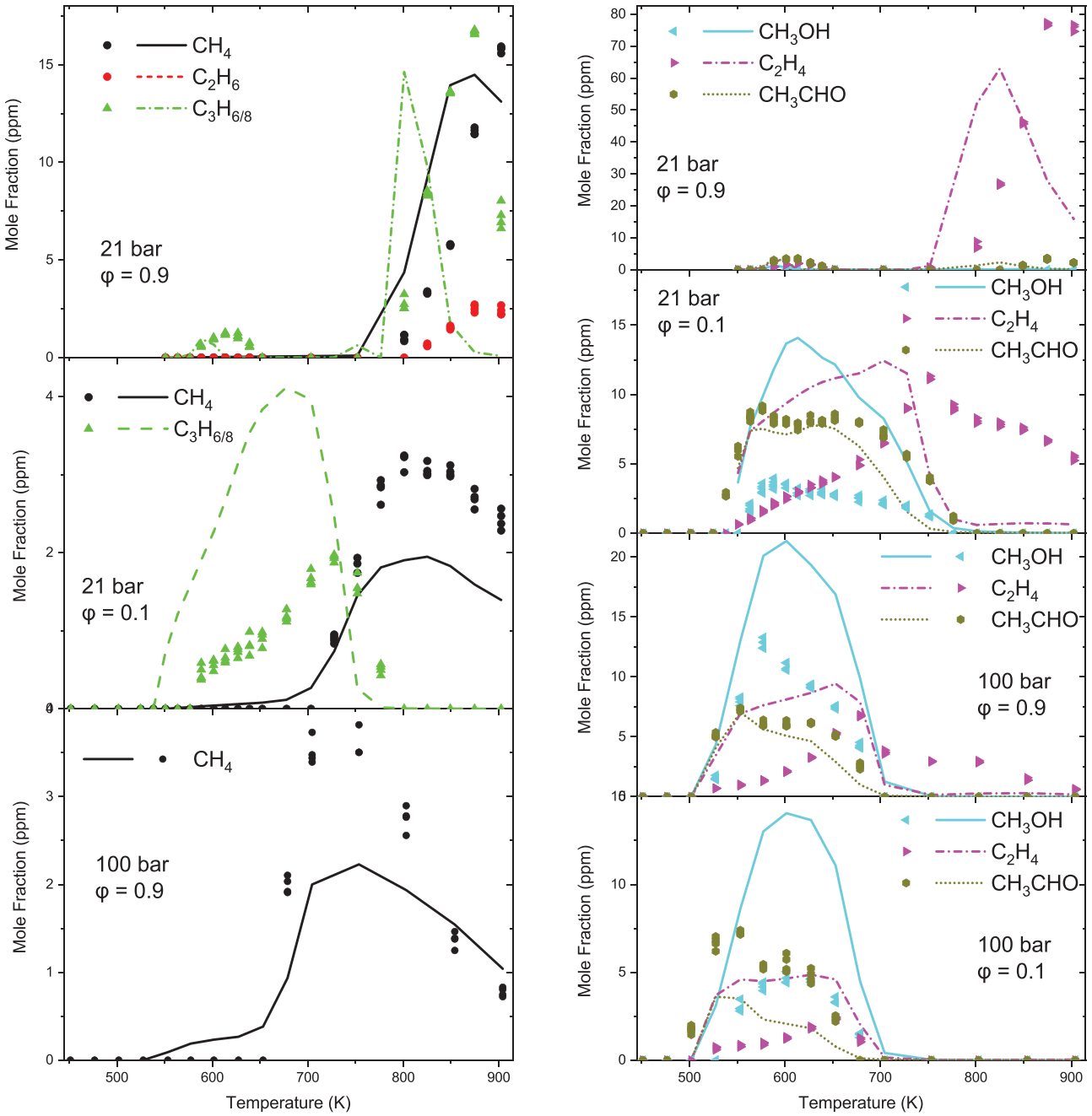

FIGURE 4 Comparison of the measured mole fractions of detected intermediates in the flow reactor as a function of temperature, pressure, and stoichiometry with predictions from the kinetic model of Zhang et al.[9] Symbols denote experimental results, while lines correspond to modeling predictions. Mixture compositions are listed in Table 2. Concentrations of methane, ethane, or propane/propene at 100 bar lean conditions were below the detection limit. The temperature refers to the temperature profiles in Figure 1

3.2.3 | CO and CO_2

Figure 5 shows the formation of CO and CO_2. Similar to the results for *n*-heptane, there is a clear distinction between a low temperature and a high temperature region. At 21 bar and stoichiometric conditions, the only set with a pronounced NTC behavior, CO and CO_2 are observed only at high temperatures. For the other three conditions, there is a transition region at 550–650 K with a plateau in the CO and CO_2 mole fractions. Above 650 K, CO increases rapidly with temperature, reaching a peak value before being partly converted to CO_2.

Predictions with the model by Zhang et al.[9] generally compares well with the experimental data. The best agreement is at 21 bar lean conditions, while the model tends to slightly overpredict CO and underpredict CO_2 at 100 bar. At 21 bar and stoichiometric conditions, the premature high temperature oxidation of *n*-heptane (Figure 3)

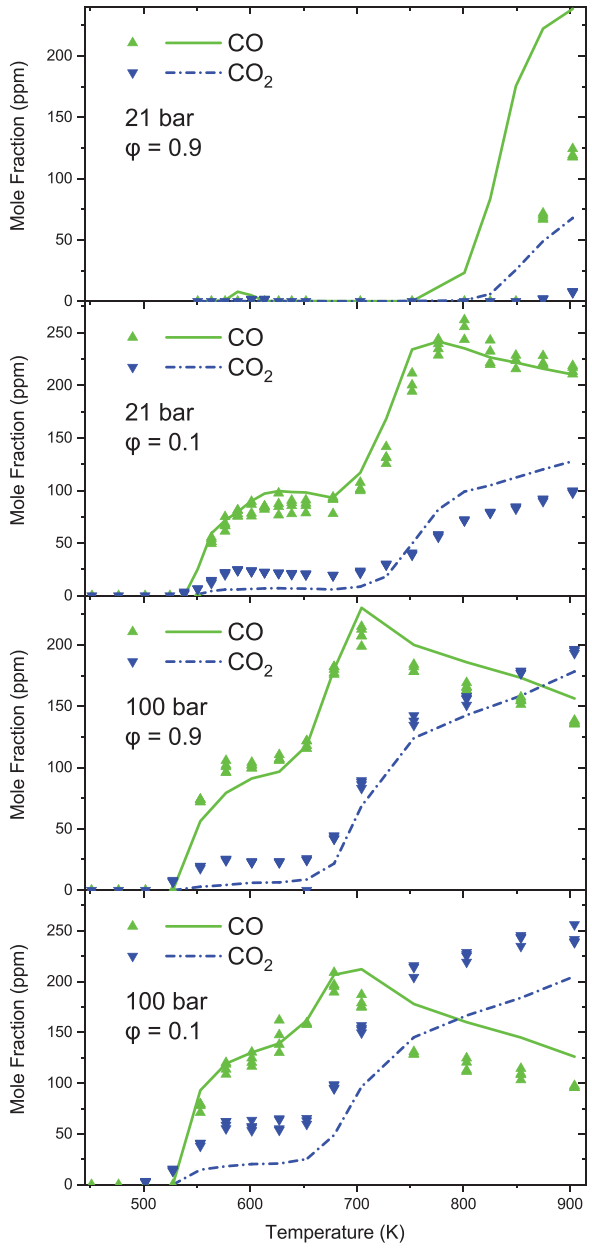

FIGURE 5 Comparison of the measured mole fractions of CO and CO_2 in the flow reactor as a function of temperature, pressure, and stoichiometry with predictions from the kinetic model of Zhang et al.[9] Symbols denote experimental results, while lines correspond to modeling predictions. Mixture compositions are listed in Table 2. The temperature refers to the temperature profiles in Figure 1

results in overprediction of the CO and CO_2 formation.

3.3 | Reaction path and sensitivity analysis

Figure 6 highlights the major reaction paths at 21 bar for the *n*-heptane oxidation according to the model by Zhang et al.[9] Oxidation proceeds through four heptyl isomers, but for clarity, the figure only details those of the 2-heptyl radical. More comprehensive reaction path diagrams are shown in the Supplementary Material. Low and high temperature pathways are distinguished in Figure 6, derived from calculations at 601 and 903 K, respectively, and 21 bar. The low temperature pathway involves an O_2 addition to the heptyl radical and proceeds mainly through cyclic ether formation, even though also keto-hydroperoxide formation plays a role at these conditions. The keto-hydroperoxide pathway is chain branching with the production of two OH radicals, whereas the cyclic ether pathway is chain propagating with one OH being reproduced in the cyclic ether formation. Yet, the radical pool is maintained in the further decomposition by the formation of HO_2 radicals.

The cyclic ether (C_7H_{14}O-2,5) is consumed mainly by reaction with OH to form linear oxygenated intermediates that are converted further to C_2 species such as ethene and ketene. Depending on the pathway, either propene (C_3H_6) or butene (1-C_4H_8) are formed by elimination. The keto-hydroperoxide (C_7H_{14}O-4OOH) decomposes through a keto-alkoxy radical after an OH elimination, also to form linear oxygenated intermediates, including an aldehyde. Decomposition of the oxygenated C_2 species eventually yields methyl radicals (CH_3), which to a significant extent recombine with O_2 to form CH_3OO. The peroxide radical then reacts with OH or HO_2 to form methanol or CH_3OOH, respectively, with CH_3OOH eventually converted to methanol or formaldehyde.

The high temperature pathway in Figure 6 involves mainly thermal decomposition of the heptyl radical into smaller hydrocarbons, eventually forming ethene. The formation of acetaldehyde at these conditions origins from a cyclo-propyl radical (C_3H_5-S), which is an intermediate product of the thermal decomposition of *n*-heptane. Acetaldehyde is mainly converted through the methyl radical, forming methane by reaction with HO_2. The methanol formed at elevated temperature is less stable than methane and is largely oxidized to CO and CO_2.

The diagrams in the Supplementary Material allow a comparision of the oxidation paths of the four heptyl radicals. At low temperatures, the cyclic ether formation is the dominating path for 1-C_7H_{15}, 2-C_7H_{15}, and 3-C_7H_{15} while reaction through keto-hydroperoxide is the main path for 4-C_7H_{15}, as the primary internal hydrogen abstraction is less-favored. Under fuel lean conditions, the keto-hydroperoxide paths are enhanced due to the increased rate of the second O_2 addition; this results in a higher conversion of *n*-heptane. At higher temperatures, all the heptyl radicals decompose thermally into alkenes and alkyl radicals. The formation of the alkyl radical with the largest carbon chain is favored in the 3-C_7H_{15} decomposition

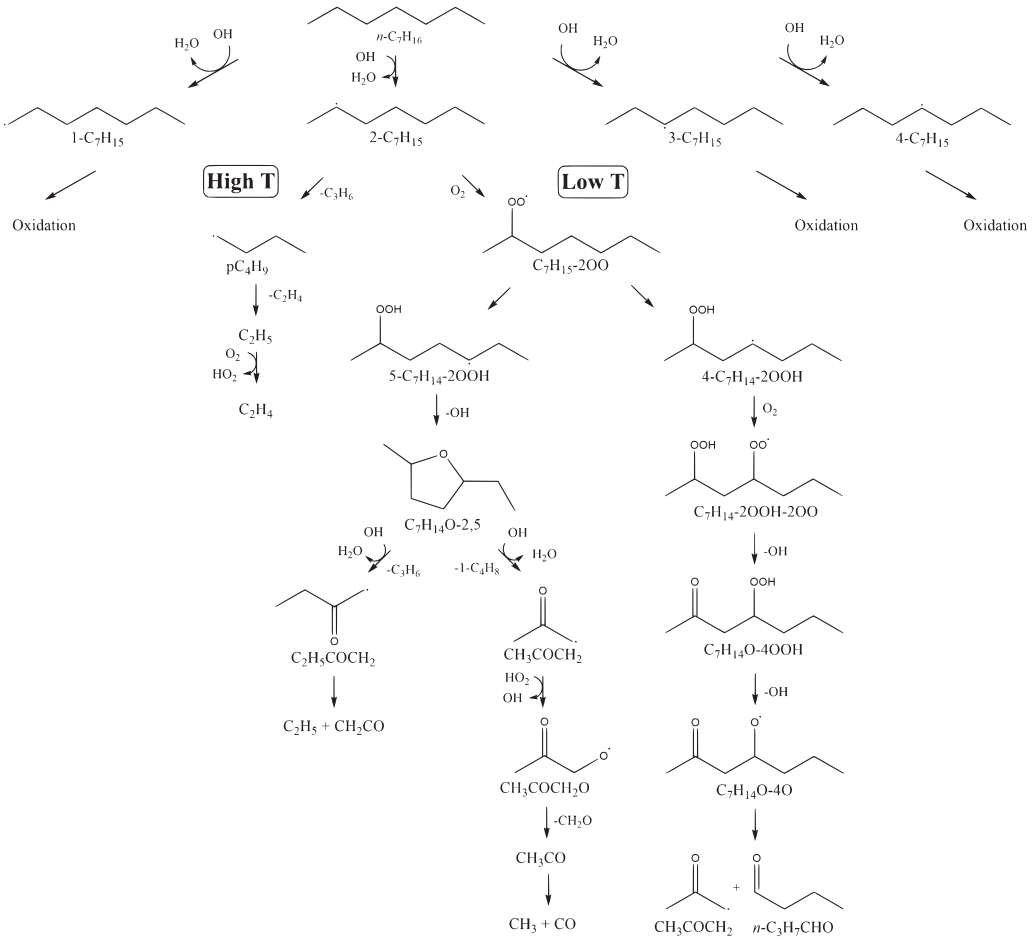

FIGURE 6 Major reaction pathways for *n*-heptane decomposition at low (601 K temperature profile) and high temperatures (903 K temperature profile), respectively, according to the model by Zhang et al.[9] Pressure is 21 bar and conditions are stoichiometric. The diagram is based on the rate of production (ROP) at the halfway point toward the final *n*-heptane conversion for the given temperature profile

Figure 7 shows a sensitivity analysis for *n*-heptane at 21 bar and near-stoichiometric conditions. Negative coefficients indicate enhanced oxidation of *n*-heptane, while reactions with positive coefficients inhibit the conversion. The initial conversion is mainly controlled by reaction with OH at low temperature, and with both OH and HO_2 at higher temperatures. The hydrogen abstraction by OH occurring at the 3rd position (nC_7H_{16} + OH ⇔ 3-C_7H_{15} + H_2O) shows up as an inhibiting step, as the reaction sequence this isomer is less reactive than those of 1-C_7H_{15} and 2-C_7H_{15}. The larger sensitivity to HO_2 reactions at higher temperatures is related to the importance of the H_2O_2 decomposition and the methyl oxidation (CH_3 + HO_2). In general, the low temperature oxidation is sensitive to the peroxy chemistry (ROO, ROOH, QOOH, etc.), where the terminating steps involve ROO forming olefins and HO_2. In particular, the second O_2 additions exhibit large sensitivity coefficients, inhibiting or enhancing the *n*-heptane oxidation.

The high temperature chemistry is sensitive to reactions from the hydrogen subset involving HO_2, H_2O_2, and OH, as well as their reactions with the methyl radical and *n*-heptane. Sensitivity coefficients at 775 and 900 K are similar. The overprediction of the conversion of *n*-heptane in Figure 3 indicates that the model does not capture the balance between low and high temperature pathways correctly at 776 K.

4 | CONCLUSION

Novel high-pressure (21–100 bar) *n*-heptane oxidation experiments in a laminar flow reactor have been conducted under near-stoichiometric and fuel-lean conditions, and at temperatures of 450–900 K. Concentrations of reactants, selected intermediates, and products were quantified by a GC. An NTC region was clearly observed at 21 bar and Φ = 0.9, starting at 600 K. At higher pressures and/or higher oxygen levels, the NTC behavior was less pronounced.

The measured species profiles were compared to predictions with selected literature mechanisms. Even though

INTERNATIONAL JOURNAL OF CHEMICAL KINETICS WILEY

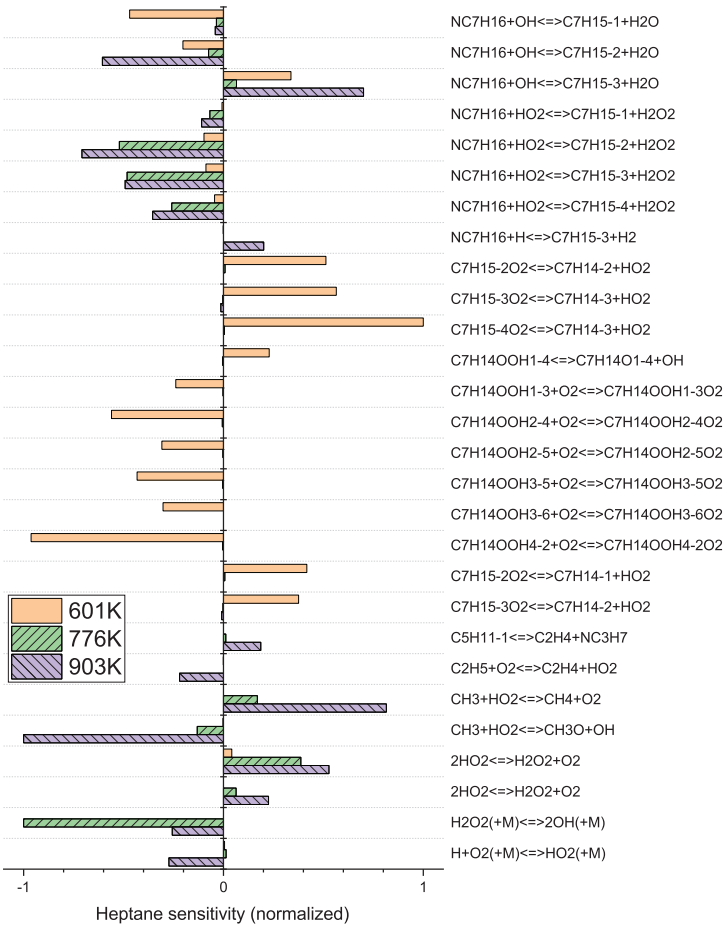

FIGURE 7 Normalized sensitivity coefficients for the predicted *n*-heptane mole fraction at 21 bar and stoichiometric conditions at temperature profiles of 601, 776, and 903 K. The sensitivity coefficients are obtained at a halfway point toward the final *n*-heptane conversion for the given temperature profile. Separated graphs are shown in the Supplementary Material Figures S5–S7

almost all the models had been validated against ignition delay data obtained at elevated pressure and intermediate temperatures, only the models from Zhang et al.[9], Wu et al.[21], and Ranzi et al.[23] were able to capture the observed NTC behavior. This shows the value of the present experimental results for further validation and development of the detailed *n*-heptane models. The best overall agreement for *n*-heptane oxidation was obtained with the model by Zhang et al.[9] A reaction path analysis showed low temperature pathways involving the formation of heptyl peroxy radicals and cyclic ethers, while at higher temperatures, *n*-heptane decomposes thermally into smaller hydrocarbons, eventually forming ethene.

ACKNOWLEDGMENTS

The work has been conducted at the CHEC (Combustion and Harmful Emission Control) research center at DTU Chemical Engineering with funding from the Independent Research Fund Denmark (IRFD).

DATA AVAILABILITY STATEMENT

The data that supports the findings of this study are available in the supplementary material of this article.

ORCID

Lauge Sven Thorsen https://orcid.org/0000-0002-5495-7874
Hamid Hashemi https://orcid.org/0000-0002-1002-0430
Peter Glarborg https://orcid.org/0000-0002-6856-852X

REFERENCES

1. Ciezki HK, Adomeit G. Shock-tube investigation of self-ignition of n-heptane-air mixtures under engine relevant conditions. *Combust Flame*. 1993;93:421-433.
2. Fieweger K, Blumenthal R, Adomeit G. Self-ignition of S.I. engine model fuels: a shock tube investigation at high pressure. *Combust Flame*. 1997;109:599-619.
3. Gauthier BM, Davidson DF, Hanson RK. Shock tube determination of ignition delay times in full-blend and surrogate fuel mixtures. *Combust Flame*. 2004;139:300-311.
4. Herzler J, Jerig L, Roth P. Shock tube study of the ignition of lean n-heptane/air mixtures at intermediate temperatures and high pressures. *Proc Combust Inst*. 2005;30:1147-1153.
5. Shen HPS, Steinberg J, Vanderover J, Oehlschlaeger MA. A Shock tube study of the ignition of n-heptane, n-decane, n-dodecane, and n-tetradecane at elevated pressures. *Energy Fuels*. 2009;23:2482-2489.

6. Heufer KA, Olivier H. Determination of ignition delay times of different hydrocarbons in a new high pressure shock tube. *Shock Waves*. 2010;20:307-316.
7. Dagaut P, Reuillon M, Cathonnet M. Experimental study of the oxidation of n-heptane in a jet stirred reactor from low to high temperature and pressures up to 40 atm. *Combust Flame*. 1995;101:132-140.
8. Herbinet O, Husson B, Serinyel Z, et al. Experimental and modeling investigation of the low-temperature oxidation of n-heptane. *Combust Flame*. 2012;159:3455-3471.
9. Zhang K, Banyon C, Bugler J, et al. An updated experimental and kinetic modeling study of n-heptane oxidation. *Combust Flame*. 2016;172:116-135.
10. Griffiths J, Halford-Maw P, Rose D. Fundamental features of hydrocarbon autoignition in a rapid compression machine. *Combust Flame*. 1993;95:291-306.
11. Minetti R, Carlier M, Ribaucour M, Therssen E, Sochet LR. A rapid compression machine investigation of oxidation and autoignition of n-heptane: measurements and modeling. *Combust Flame*. 1995;102:298-309.
12. Griffiths JF, Halford-Maw PA, Mohamed C. Spontaneous ignition delays as a diagnostic of the propensity of alkanes to cause engine knock. *Combust Flame*. 1997;111:327-337.
13. Silke EJ, Curran HJ, Simmie JM. The influence of fuel structure on combustion as demonstrated by the isomers of heptane: a rapid compression machine study. *Proc Combust Inst*. 2005;30II:2639-2647.
14. Karwat DM, Wagnon SW, Wooldridge MS, Westbrook CK. Low-temperature speciation and chemical kinetic studies of n-heptane. *Combust Flame*. 2013;160:2693-2706.
15. Callahan CV, Held TJ, Dryer FL, et al. Experimental data and kinetic modeling of primary reference fuel mixtures. *Symp Int Combust*. 1996;26:739-746.
16. Lenhert DB, Miller DL, Cernansky NP, Owens KG. The oxidation of a gasoline surrogate in the negative temperature coefficient region. *Combust Flame*. 2009;156:549-564.
17. Curran HJ, Gaffuri P, Pitz WJ, Westbrook CK. A comprehensive modeling study of n-heptane oxidation. *Combust Flame*. 1998;114:149-177.
18. Mehl M, Pitz WJ, Westbrook CK, Curran HJ. Kinetic modeling of gasoline surrogate components and mixtures under engine conditions. *Proc Combust Inst*. 2011;33:193-200.
19. Seidel L, Moshammer K, Wang X, Zeuch T, Kohse-Höinghaus K, Mauss F. Comprehensive kinetic modeling and experimental study of a fuel-rich, premixed n-heptane flame. *Combust Flame*. 2015;162:2045-2058.
20. Cai L, Pitsch H. Optimized chemical mechanism for combustion of gasoline surrogate fuels. *Combust Flame*. 2015;162:1623-1637.
21. Wu Y, Panigrahy S, Sahu AB, et al. Understanding the antagonistic effect of methanol as a component in surrogate fuel models: a case study of methanol/n-heptane mixtures. *Combust Flame*. 2021;226:229-242.
22. Ranzi E, Frassoldati A, Stagni A, Pelucchi M, Cuoci A, Faravelli T. Reduced kinetic schemes of complex reaction systems: fossil and biomass-derived transportation fuels. *Int J Chem Kinet*. 2014;46:512-542.
23. Ranzi E, Cavallotti C, Cuoci A, Frassoldati A, Pelucchi M, Faravelli T. New reaction classes in the kinetic modeling of low temperature oxidation of n-alkanes. *Combust Flame*. 2015;162:1679-1691.
24. Bernardi M, Pelucchi M, Stagni A, et al. Curve matching, a generalized framework for models/experiments comparison: an application to n- heptane combustion kinetic mechanisms. *Combust Flame*. 2016;168:186-203.
25. Bagheri G, Ranzi E, Pelucchi M, Parente A, Frassoldati A, Faravelli T. Comprehensive kinetic study of combustion technologies for low environmental impact: MILD and OXY-fuel combustion of methane. *Combust Flame*. 2020;212:142-155.
26. Campbell MF, Wang S, Davidson DF, Hanson RK. Shock tube study of normal heptane first-stage ignition near 3.5 atm. *Combust Flame*. 2018;198:376-392.
27. Davis S, Law C. Laminar flame speeds and oxidation kinetics of iso-octane-air and n-heptane-air flames. *Symp Int Combust*. 1998;27:521-527.
28. Kumar R, Singhal A, Katoch A, Kumar S. Experimental investigations on laminar burning velocities of n-heptane + air mixtures at higher mixture temperatures using externally heated diverging channel method. *Energy Fuels*. 2020;34:2405-2416.
29. Held TJ, Marchese AJ, Dryer FL. A semi-empirical reaction mechanism for n-heptane oxidation and pyrolysis. *Combus Sci Technol*. 1997;123:107-146.
30. Rasmussen CL, Hansen J, Marshall P, Glarborg P. Experimental measurements and kinetic modeling of CO/H2/O2/NOx conversion at high pressure. *Int J Chem Kinet*. 2008;40:454-480.
31. Hashemi H, Christensen JM, Harding LB, Klippenstein SJ, Glarborg P. High-pressure oxidation of propane. *Proc Combust Inst*. 2019;37:461-468.
32. ANSYS. *Chemkin-Pro Reaction Workbench 2020 R2*. ANSYS, Inc.; 2020.

SUPPORTING INFORMATION

Additional supporting information can be found online in the Supporting Information section at the end of this article.

How to cite this article: Thorsen LS, Jensen MST, Pullich MS, Christensen JM, Hashemi H, Glarborg P. *n*-Heptane oxidation in a high-pressure flow reactor. *Int J Chem Kinet*. 2022;54:669–678. https://doi.org/10.1002/kin.21604